INSTITUTE OF PHYSICS PUBLISHING JOURNAL OF PHYSICS B: ATOMIC, MOLECULAR AND OPTICAL PHYSICS

J. Phys. B: At. Mol. Opt. Phys. **36** (2003) 1337–1350 PII: S0953-4075(03)56701-3

Electron-impact excitation of B^+ using the *R*-matrix with pseudo-states method

N R Badnell[1], D C Griffin[2] and D M Mitnik[2,3]

[1] Department of Physics, University of Strathclyde, Glasgow G4 0NG, UK
[2] Department of Physics, Rollins College, Winter Park, FL 32789, USA

Received 25 November 2002, in final form 27 January 2003
Published 14 March 2003
Online at stacks.iop.org/JPhysB/36/1337

Abstract

We have carried out several *R*-matrix with pseudo-states (RMPS) calculations for the electron-impact excitation of B^+. Maxwell-averaged effective collision strengths have been determined for excitations between the lowest 20 terms, including all those arising from the 2s3*l* and 2s4*l* configurations. A comparison of results from 114 term and 134 term close-coupling (CC) RMPS calculations demonstrates the convergence in the pseudo-state expansion representing the continuum and high bound-states. Comparison of the 114CC RMPS results with those from a 20CC *R*-matrix calculation, using the same 114 term configuration interaction target, shows a reduction in the effective collision strengths by up to a factor of two at higher temperatures for transitions to $n = 4$. The modelling of spectral emission from boron, and from $n = 4$ terms in B^+ in particular, is important for studying impurity influx in both current (TEXTOR) and future (ITER) magnetic fusion reactors.

1. Introduction

Light elements ($Z \leqslant 10$) are present in magnetic fusion plasmas from a variety of sources: Li beams are introduced so as to study transport; Be, B and C are used as facing materials for the divertor and reactor walls; Ne is used in the divertor to cool the plasma; N and O are ever-present impurities, while H and He are there as a matter of course. Spectral modelling of these light impurities tells us about their distribution within the plasma and, hence, gives insight into the mechanisms of their ingress; namely transport, wall erosion and divertor confinement, or lack thereof. Electron-impact excitation is a significant, and often the dominant, populating process of the radiating levels.

In recent years, calculations using the convergent close-coupling (CCC) (Bray and Stelbovics 1992) and *R*-matrix with pseudo-states (RMPS) (Bartschat *et al* 1996, Badnell and Gorczyca 1997) methods have clearly demonstrated the importance of coupling to the target continuum and high bound-states on electron-impact excitation in neutral atoms and

[3] Present address: Departamento de Física, FCEN, Universidad de Buenos Aires, Buenos Aires, Argentina.

0953-4075/03/071337+14$30.00

low-charge ions. In particular, the application of the RMPS method to H- and Li-like ions so as to generate Maxwell-averaged data for modelling purposes is now almost routine; see, e.g., Anderson *et al* (2000a, 2000b), Ballance *et al* (2003a) and Griffin *et al* (2000, 2001). Moving to He-like ions doubles the number of target states included in the CC calculations, increasing the computational time by a factor of $\sim$10. Furthermore, data for application purposes require that the underlying cross sections be computed over a wide range of angular momenta and energies. Such results for He have been presented by Bray *et al* (2000) (CCC) and for Li^+ by Ballance *et al* (2003b) (RMPS).

The move to Be-like ions is even more computationally demanding. As in the case of He-like ions, the size of the RMPS calculations becomes inflated, compared to H- and Li-like, because of the presence of both singlet and triplet terms in the pseudo-state basis that is used to represent the high bound-states and the target continuum. But now we must consider 2snl *and* 2pnl target expansions, which give rise to almost a further factor of 4 increase in the number of terms since for each 2snl SL term with $L = l$ there are three 2pnl SL' terms, corresponding to $L' = l - 1, l, l + 1$, in general. Our first RMPS calculation for a Be-like ion was for C^{2+} (see Mitnik *et al* 2003), which has long been a magnetic fusion diagnostic, as well as being of astrophysical importance. The largest RMPS calculation for C^{2+} by Mitnik *et al* (2003) included 238 CC terms and resulted in $(N + 1)$-electron Hamiltonian matrices of rank up to 36 000. Diagonalization of these matrices benefited significantly from the use of our parallel *R*-matrix programs.

Data for the electron-impact excitation of B^+ are of importance for diagnosing magnetic fusion plasmas. Boronization of surfaces is under study for utilization in the next generation of reactors (e.g. ITER). Currently, boron is used as a facing in the TEXTOR reactor at Jülich in Germany. Four lines have been observed, including two originating from $n = 4$ terms (Borodine 2002). There does not appear to be much in the way of previous excitation data for B^+. Data currently used for modelling are from a plane-wave Born calculation (O'Mullane 2002). It is clear from previous RMPS calculations that excitation of the $n = 4$ terms will require an RMPS calculation. Omission of coupling to the continuum can result in Maxwell-averaged data being a factor of two too large. We investigate this for B^+ by carrying out pseudo-state and non-pseudo-state *R*-matrix calculations. We also carry out several RMPS calculations so as to determine the sensitivity to the pseudo-state expansion. Because so few terms from 2pnl are bound in B^+, compared to C^{2+}, we do not need so large a CC expansion as Mitnik *et al* (2003). However, the spectroscopic atomic structure is more problematic for this single ionized atom than for C^{2+}.

The remainder of this paper is organized as follows. In the next section, we discuss the spectroscopic and pseudo-states that we used to represent the bound and continuum target terms. In section 3, we describe the details of our pseudo-state and non-pseudo-state scattering calculations, which utilize our suite of parallel *R*-matrix programs. In section 4, we present illustrative results from our calculations. Finally, we conclude in section 5 with a summary of our findings.

2. Structure

2.1. Background

The approach to a traditional (i.e. non-RMPS) collision calculation is to first determine the atomic structure to high accuracy, e.g. in energies and oscillator strengths. In other words, the N-electron problem is largely converged, at least for the few low-lying spectroscopic atomic states for which collision data are to be generated. Often, use is made of a small number of pseudo-states which are optimized solely on the few low-lying spectroscopic states. The accuracy of the $(N + 1)$-electron collision problem solved next is then mainly a function of the

importance of coupling to the continuum and high bound-states. Except at low energies, this accuracy is poor for low-charge ions.

The N- and $(N + 1)$-electron problems are more closely entwined in the case of pseudo-state CC calculations for complex ions. Here, we require a single complete basis for the target which gives an accurate representation of the low-lying spectroscopic states as well as a good representation of high bound-states and the continuum. Such a representation is provided for by the use of Laguerre pseudo-states. These form a quadrature for the sum over high bound-states and the integral over continuum states found in the CC expansion. In this instance, we have little freedom in optimizing pseudo-orbitals since we do not wish to prejudice one part of our representation for another. Obviously, in the converged limit, our pseudo-state expansion provides an accurate representation of the entire N-electron spectrum. In practice, the size of pseudo-state expansion that it is practical to work with and which gives a reasonable representation of high bound-states and the continuum does not give quite such a good representation of low-lying spectroscopic states as we are used to seeing when we had the freedom to optimize our pseudo-states solely there. We seek to assess the impact that this may have on the accuracy of our collision data.

2.2. Previous work

There have been a number of studies on the atomic structure of B^+, but most of the focus has been on the $n = 2$ complex. Large-scale calculations have been carried out by Jönsson *et al* (1999) using the multi-configuration Hartree–Fock (MCHF) method and by Zhu and Chung (1995) using the full-core plus correlation (FCPC) method. The two sets of results are in close agreement. Two other papers are of note, both from the Opacity Project. Fernley *et al* (1999) generated radiative data for B-like ions utilizing an R-matrix scattering calculation for Be-like ions. The work of Tully *et al* (1990) was for radiative data for Be-like ions, which were obtained utilizing an R-matrix scattering calculation for Li-like ions. The Be-like targets of Fernley *et al* (1999) were obtained from the program CIV3 and made use of pseudo-orbitals which were optimized so as to improve the accuracy of the description of the $n = 2$ ground complex. Their subsequent R-matrix calculation only included the $n = 2$ complex in the CC expansion. We can follow the procedure of Fernley *et al* (1999), but with AUTOSTRUCTURE, and produce results that are similar to theirs. However, there is no way that we can extend this approach to include a representation of the continuum at the same time. We also require spectroscopic orbitals through to $n = 4$. The approach of Tully *et al* (1990) is to use a simple Li-like target (2s, 2p, 3s, 3p, 3d) and then to solve the CC scattering equations for the Be-like system for closed channels, obtaining energy levels and oscillator strengths. If we carry out a large-scale pseudo-state expansion of the form $2s\bar{n}l$ and $2p\bar{n}l$ for the target and diagonalize the N-electron Hamiltonian then formally, in the limit of large $\bar{n}$, we would approach the results of the R-matrix expansions $2skl$ and $2pkl$. In general though, the R-matrix expansions used are much denser than the pseudo-state expansions and are fully converged, over a finite energy range.

The R-matrix oscillator strengths of Tully *et al* (1990) are in slightly better agreement with those of the MCHF and FCPC methods than are those from CIV3 obtained by Fernley *et al* (1999)—see Fernley *et al* for a detailed comparison for the $n = 2$ complex. We will compare our oscillator strengths with those of Tully *et al* (1990) since we wish to assess the accuracy of our description of the $n = 3$ and 4 terms.

2.3. Results

All of the target orbitals in these calculations were generated using the program AUTOSTRUCTURE. The spectroscopic orbitals were determined from local potentials that are themselves

Table 1. Term energies (Ryd) for B^+.

Index	Configuration	Term	Observed[a]	This work
1	$2s^2$	^1S	0.0000	−0.0500
2	2s2p	^3P	0.3404	0.3035
3	2s2p	^1P	0.6688	0.6577
4	$2p^2$	^3P	0.9015	0.8741
5	$2p^2$	^1D	0.9328	0.9075
6	$2p^2$	^1S	1.1633	1.2059
7	2s3s	^3S	1.1826	1.1604
8	2s3s	^1S	1.2356	1.2813
9	2s3p	^3P	1.3122	1.3122
10	2s3p	^1P	1.3132	1.3032
11	2s3d	^3D	1.3728	1.3674
12	2s3d	^1D	1.4096	1.4148
13	2s4s	^3S	1.5158	1.5368
14	2s4s	^1S	1.5303	1.5354
15	2s4p	^1P	1.5545	1.5556
16	2s4p	^3P	1.5632	1.5673
17	2s4d	^3D	1.5863	1.5887
18	2s4f	^3F	1.5938	1.5979
19	2s4f	^1F	1.5940	1.5983
20	2s4d	^1D	1.5997	1.6056

determined using Slater-type orbitals (Badnell 1997), while the pseudo-orbitals were determined from Laguerre polynomials (Badnell and Gorczyca 1997).

The first thing that we note is that most terms in B^+ resulting from 2pnl ($n > 2$) lie above the ionization limit. Only some of the terms from 2p3l lie just below the ionization limit and these are intermixed with terms from 2snl, for $n \geqslant 5$. Spectroscopic modelling for fusion takes place on lower-lying terms, up to 2s4l SL. Apart from the $n = 2$ complex, all transitions of interest are of the form 2s$nl \rightarrow 2sn'l'$. Consequently, there is little need to represent coupling to high bound-states and the continuum attached to 2p. (Transitions between 2s2p $\rightarrow$ $2p^2$ only couple weakly to the continuum.) Thus, we first consider a spectroscopic plus pseudo-state configuration interaction (CI) expansion 2snl up to $nl = 10$g and 2pnl up to $nl = 5$g. This results in a total of 114 terms. Based on past experience, we initially used spectroscopic orbitals up to 3d and pseudo-orbitals from thereon. The reason for this choice is that Laguerre pseudo-orbitals are more spatially compact than spectroscopic ones and this enables us to use a smaller R-matrix box size. However, it still results in 2s4l SL terms that are a good representation of the spectroscopic ones, based on a comparison of energy levels with observed and oscillator strengths with those from Tully *et al* (1990). If instead we use spectroscopic $n = 4$ orbitals determined from the Slater potentials then we find that the resulting oscillator strengths from the 2s4l terms are not quite as accurate. Of course, in both cases, diagonalization of the N-electron Hamiltonian induces configuration mixing which corrects for the initially quite different $n = 4$ orbitals.

In table 1, we compare our term energies for the 20 lowest-lying terms with observed energies, taken from the NIST Atomic Spectra Database[4]. We see that the computed position for the $2p^2$ ^1S term is above the 2s3s ^3S, rather than below. Also, we see that the remaining excited term energies are typically ≈0.05 Ryd too high. We adjust the position of our calculated

[4] NIST webpage: http://physics.nist.gov

terms to the observed positions in the scattering calculation. (Since the terms whose positions are interchanged do not interact, interchanging is no different from shifting terms by a similar amount but not interchanging.) However, terms 9–20 are consistently 0.040–0.056 Ryd too high relative to the ground term. Also, the difference for terms 2–8 is in the same direction, but varying between 0.013 and 0.096 Ryd. Thus, our shifts are not as significant as might initially be thought. These shifts in threshold improve the position of resonances attached to them, excluding the correlation resonances.

In table 2, we compare our symmetric oscillator strengths (gf) from the $n = 2$ complex with those from the R-matrix bound-state calculations of Tully *et al* (1990). On the whole, the level of agreement for the length form is quite good—the strong transitions (>0.01) agree to within 20%, apart from the transitions 2s2p ^{1}P–2s4s ^{1}S (0.0149 versus 0.0105) and 2p^2 ^{1}S–2s4p ^{1}P (0.225 versus 0.131), but the latter involves a two-electron jump. Our velocity results tell us little new. For some transitions (3–8, 4–16) we obtain good agreement between length and velocity but poor agreement with Tully *et al* (1990). For other transitions (2–7, 3–6, 5–10), we obtain poor agreement between our length and velocity results but good agreement between our length results and those of Tully *et al* (1990). We also compared these (table 2) energies and oscillator strengths with those that we obtained using the 4l orbitals that were generated from Slater potentials for our zero-order basis, but we found no improvement in the agreement. In addition, we looked at allowed transitions involving a one-electron jump from the 2p^2 ^{1}S term (to 2p3l) and found a similar level of agreement with Tully *et al* (1990) as we have already observed for the one-electron transitions in table 2.

3. Collision calculations

3.1. Codes

The collision calculations were carried out with our parallel versions of the RMATRX1 suite of programs. The recently parallelized PSTG1 and PSTG2 codes have been described by Mitnik *et al* (2003) while our longer standing PSTG3 and PSTGF codes are described in Mitnik *et al* (2001). PSTG1, PSTG2 and PSTG3 solve the CC equations in the R-matrix inner region while PSTGF solves them in the outer region. The PSTG1 code incorporates the rigorous RMPS approach of Badnell and Gorczyca (1997), specifically, the formation of a single linearly independent basis from a large pseudo-state basis and the R-matrix continuum basis, including the appropriate transformation of the Buttle correction. PSTG2 and PSTG3 incorporate the approach of Gorczyca *et al* (1995) to form a correctly balanced (N + 1)-electron bound–bound expansion when differing CI and CC expansions are used. Finally, PSTGF initially solves uncoupled equations and then treats the coupling terms as a perturbation, both accurately and efficiently.

3.2. Set-up

We have carried out four CC calculations. The first was a 114CC RMPS calculation using the N-electron expansion (to 10g) described previously. This expansion had four configurations per l of the form 2s$\bar{n}l$ lying in the continuum, one with terms lying a little above the position of the physical $n = 5$ terms and one ($\bar{n} = 6$) with terms distributed around the ionization limit. These $n = 5$ (and $\bar{n} = 6$) terms approximate the important coupling to spectroscopic 2s5l SL terms at low energies (e.g. resonances) as well as higher 2snl SL terms. The spectroscopic 2p4l and 2p5l states lie above the ionization limit and are treated along with all other continuum coupling. To assess the sensitivity to the bound and continuum expansion, we also carried out a 134CC RMPS calculation resulting from the addition of 2s$\bar{n}l$ configurations for $\bar{n} = 11$, 12

Table 2. Symmetric oscillator strengths (gf) for selected transitions in B^+.

			This work		
i	j	Transition	Velocity	Length	Tully *et al* (1990)
1	3	$2s^2\ ^1S$–$2s2p\ ^1P$	1.01	1.03	1.03
1	10	$2s^2\ ^1S$–$2s3p\ ^1P$	0.105	0.113	0.099
1	15	$2s^2\ ^1S$–$2s4p\ ^1P$	0.0454	0.0498	0.0512
2	4	$2s2p\ ^3P$–$2p^2\ ^3P$	3.13	3.26	3.19
2	7	$2s2p\ ^3P$–$2s3s\ ^3S$	0.703	0.556	0.580
2	11	$2s2p\ ^3P$–$2s3d\ ^3D$	4.42	4.46	4.32
2	13	$2s2p\ ^3P$–$2s4s\ ^3S$	0.112	0.093	0.103
2	17	$2s2p\ ^3P$–$2s4d\ ^3D$	1.09	1.06	1.13
3	5	$2s2p\ ^1P$–$2p^2\ ^1D$	0.403	0.456	0.467
3	6	$2s2p\ ^1P$–$2p^2\ ^1S$	0.488	0.686	0.675
3	8	$2s2p\ ^1P$–$2s3s\ ^1S$	0.0763	0.0858	0.0397
3	12	$2s2p\ ^1P$–$2s3d\ ^1D$	1.43	1.50	1.59
3	14	$2s2p\ ^1P$–$2s4s\ ^1S$	0.0060	0.0149	0.0105
3	20	$2s2p\ ^1P$–$2s4d\ ^1D$	0.409	0.405	0.459
4	9	$2p^2\ ^3P$–$2s3p\ ^3P$	0.0163	0.0007	0.0002
4	16	$2p^2\ ^3P$–$2s4p\ ^3P$	0.0065	0.0069	0.0013
5	10	$2p^2\ ^1D$–$2s3p\ ^1P$	0.367	0.194	0.210
5	15	$2p^2\ ^1D$–$2s4p\ ^1P$	0.128	0.0843	0.0996
6	10	$2p^2\ ^1S$–$2s3p\ ^1P$	0.322	0.280	0.327
6	15	$2p^2\ ^1S$–$2s4p\ ^1P$	0.181	0.225	0.131

for $l = 0$–4. This added two more configurations per l to the 2s continuum. The spectroscopic structure (tables 1 and 2) changed little. Thirdly, we carried out another 114CC RMPS calculation, this time using the spectroscopic 4l orbitals (which were generated from Slater potentials) to represent both the 2s4l and 2p4l configurations. This enables us to assess the sensitivity of our collision data to the accuracy of the $n = 4$ spectroscopic representation. Finally, we carried out a 20CC calculation, but using the original 114 term CI expansion, so as to assess the effect of coupling to the continuum and high bound-states—the former dominates, except at low temperatures; see Griffin *et al* (2000). All calculations used the observed energies listed in table 1.

For the inner-region part of the calculation, we input up to 35 R-matrix continuum basis orbitals per orbital angular momentum. This enabled us to carry out scattering calculations up to 5 Ryd. We included exchange up to $L = 10$ and carried out non-exchange calculations up to $L = 40$. Since the effect of coupling to the continuum is negligible for high L, we used the non-exchange results from the 20CC calculation to complement the exchange results in all cases.

In the outer region, we used an energy step of 0.0002 Ryd from the first excited threshold through to 1.6 Ryd, i.e. just above the ionization limit. We then used a step of 0.005 Ryd thereon up to 5 Ryd for a grand total of 8178 energy points. STGF also 'tops up' for the contribution from $L > 40$. The dipole-allowed transitions were topped up using the method originally described by Burgess (1974) and implemented here; the non-dipole transitions were topped up assuming a geometric series in L, using energy ratios, with a special procedure for handling transitions between nearly degenerate levels based on the degenerate limiting case (Burgess *et al* 1970).

For application purposes, we Maxwell average our ordinary collision strengths so as to form effective collision strengths (Seaton 1953). The determination of high-temperature effective collision strengths is greatly facilitated by the use of infinite energy scaled collision

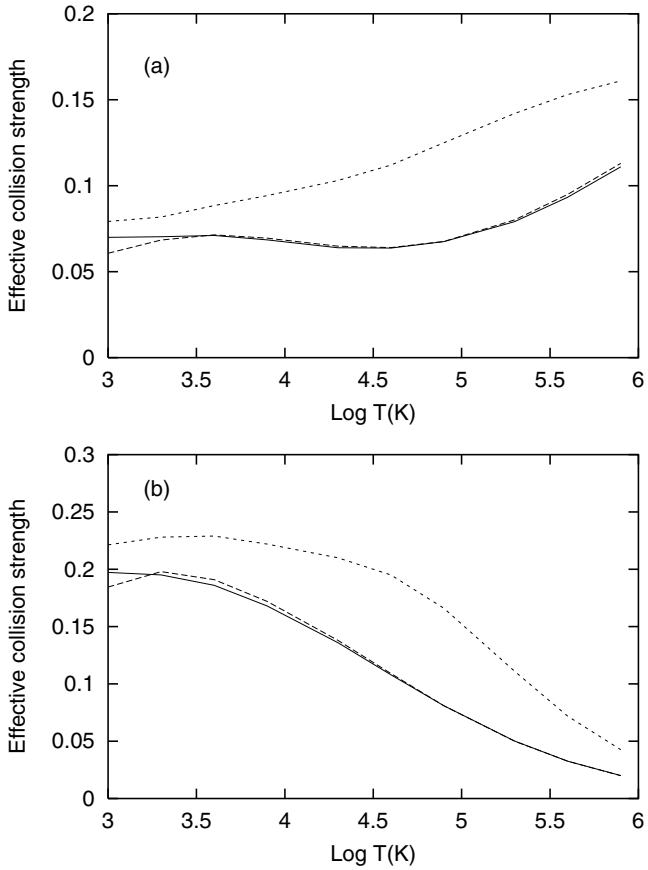

Figure 1. Effective collision strengths for excitation, from (a) the $2s^2\ ^1S$ ground term and (b) the $2s2p\ ^3P$ metastable term, to the $2s4s\ ^1S$ upper term. The dotted curves are from the present 20CC R-matrix calculation, the solid curves are from the present 114CC RMPS calculation, and the dashed curves are from the present 134CC RMPS calculation.

strengths—see Burgess and Tully (1992) and Whiteford *et al* (2001) for details. In particular, we interpolated our reduced collision strengths as a function of reduced energy between the highest energy for which calculations were performed explicitly and the infinite energy limit point. The limit value for dipole transitions is given by the Coulomb–Bethe value and that for all other spin-allowed transitions by plane-wave Born. These limit values were determined consistently using the AUTOSTRUCTURE code. Collision strengths for spin-forbidden transitions were extrapolated as $E^{-\alpha}$, with $1 < \alpha < 3$.

4. Collision results

In a dynamic fusion plasma, it is transitions from the ground and metastable terms which are of primary importance and, hence, are the main focus of our interest here.

We present effective collision strengths for temperatures between 8×10^2 and 8×10^5 K. In the coronal limit, B^+ exists over a relatively wide temperature range—it has a fractional abundance >0.5 over roughly 8×10^3–5×10^4 K (Mazzotta *et al* 1998). But in a dense,

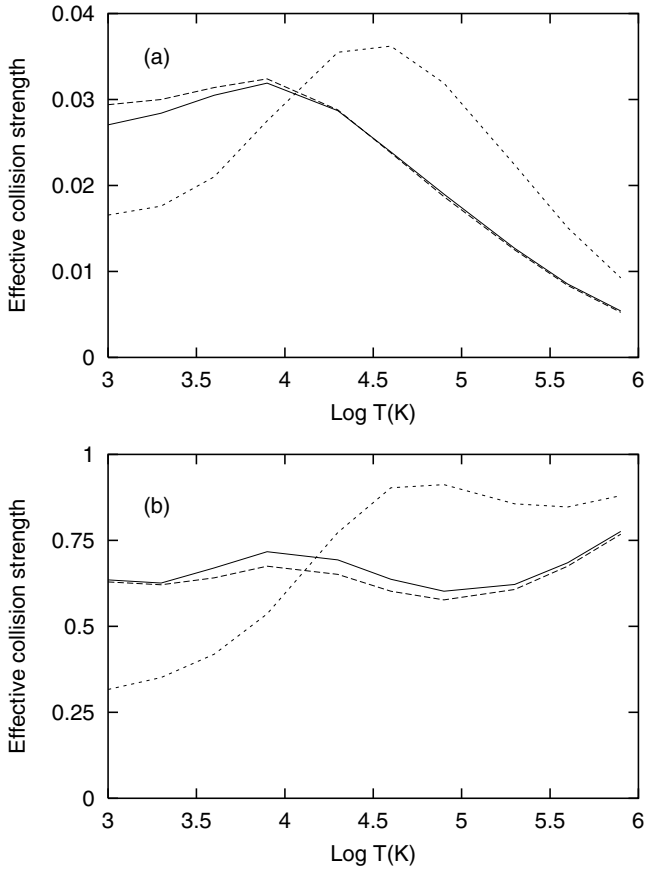

Figure 2. Effective collision strengths for excitation, from (a) the $2s^2\ ^1S$ ground term and (b) the $2s2p\ ^3P$ metastable term, to the $2s4f\ ^3F$ upper term. The dotted curves are from the present 20CC R-matrix calculation, the solid curves are from the present 114CC RMPS calculation, and the dashed curves are from the present 134CC RMPS calculation.

dynamic, fusion plasma it is necessary to be able to model the spectral emission of B^+ over an even wider temperature range. Boron atoms are sputtered off the surface of walls and move rapidly through a wide range of plasma temperatures without establishing coronal equilibrium.

4.1. To $n = 4$

We focus first on transitions from the ground and metastable terms to $2s4s\ ^1S$, $2s4f\ ^3F$ and $2s4d\ ^1D$. Radiative emission from the first two ($n = 4$) upper terms to $2s2p\ ^1P$ and $2s3d\ ^3D$, respectively, are observed at the TEXTOR magnetic fusion reactor.

In figure 1, we see that coupling to the continuum substantially reduces the effective collision strength to the $2s4s\ ^1S$ term over a wide range of temperatures, from both the ground and metastable, and that our pseudo-state expansion representing coupling to the continuum and high bound-states ($n \geqslant 5$) has converged well for these transitions (cf the 114CC and 134CC RMPS results).

In figure 2, we see that coupling to the continuum reduces the effective collision strength to the $2s4f\ ^3F$ term, from both the ground and metastable terms, but only for temperatures $T \gtrsim 10^4$ K. At lower temperatures, our RMPS results are enhanced by capture to resonances

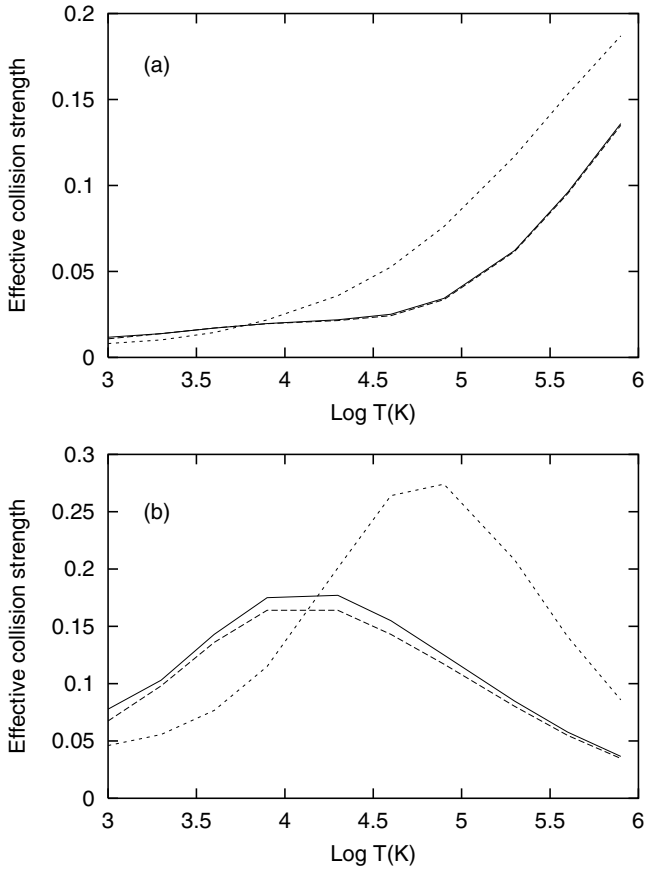

Figure 3. Effective collision strengths for excitation, from (a) the $2s^2\ ^1S$ ground term and (b) the $2s2p\ ^3P$ metastable term, to the $2s4d\ ^1D$ upper term. The dotted curves are from the present 20CC R-matrix calculation, the solid curves are from the present 114CC RMPS calculation, and the dashed curves are from the present 134CC RMPS calculation.

converging to higher ($n > 4$) thresholds represented by our bound pseudo-states. Again, there is not too much sensitivity in our results due to the pseudo-state expansion used. The low temperature ($T \sim 10^3$ K) difference starting to become apparent for the ground state is due to changes in the near-threshold resonance structure arising from the two RMPS calculations. We note that *all* resonance contributions are omitted from results obtained using distorted wave codes (e.g. ATOM) which are often used to obtain data for plasma modelling.

In figure 3, for excitation of the $2s4d\ ^1D$ term, we see a mixture of effects noted previously. From the ground term, all three sets of results are in close agreement at low temperatures, but with a reduction due to continuum coupling coming in at higher temperatures. From the metastable term, there is low temperature resonant enhancement of the RMPS effective collision strengths but, again, a substantial (factor of 2) reduction at higher temperatures due to continuum coupling.

We also compared effective collision strengths that we obtained from our two 114CC RMPS calculations, which used spectroscopic or pseudo zero-order $4l$ basis orbitals to describe the $2s4l$ and $2p4l$ configurations. We found that, at finite temperatures, differences in the effective collision strengths for dipole transitions were substantially smaller than the

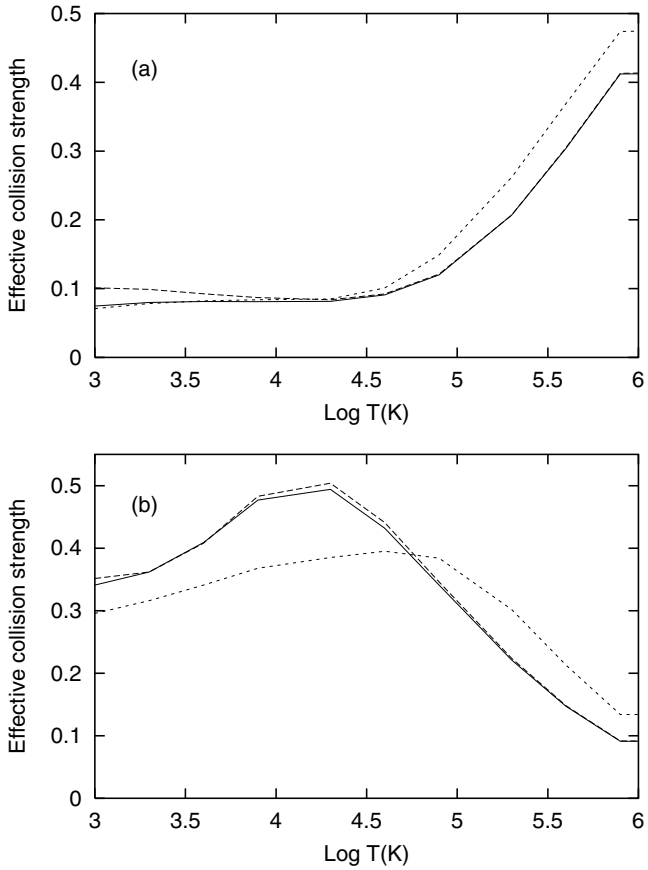

Figure 4. Effective collision strengths for excitation, from (a) the $2s^2\ ^1S$ ground term and (b) the $2s2p\ ^3P$ metastable term, to the $2s3d\ ^1D$ upper term. The dotted curves are from the present 20CC R-matrix calculation, the solid curves are from the present 114CC RMPS calculation, and the dashed curves are from the present 134CC RMPS calculation.

corresponding differences in the oscillator strengths. An extreme example: a difference of 60% in the oscillator strength for the two-electron jump 3–14 transition only resulted in a 20% difference in the effective collision strength at 2×10^4 K. Overall, results for ten transitions out of 190 differed by 30%, or more, over 8×10^2–8×10^5 K. However, only four of these involved terms with $n = 4$. In fact, these largish differences are confined to low temperatures ($<5 \times 10^3$ K) and are due to small changes in the position of near-threshold resonances. We conclude that we have a sufficiently accurate description of the 2s4l and 2p4l configurations. Finally, we adopt the results obtained utilizing the slightly more accurate (N-electron) atomic structure, as discussed in section 2.3, but care should still be exercised in using any low-temperature collision data for non-dipole transitions for which resonance contributions are large.

4.2. To $n = 3$

We expect that the effect of coupling to the continuum will be reduced on comparing the same transition, but to $n = 3$ versus 4. In figure 4, we look at results for excitation of the $2s3d\ ^1D$ term, which is the same transition as viewed in figure 3 but for $n = 3$ instead of 4. Indeed,

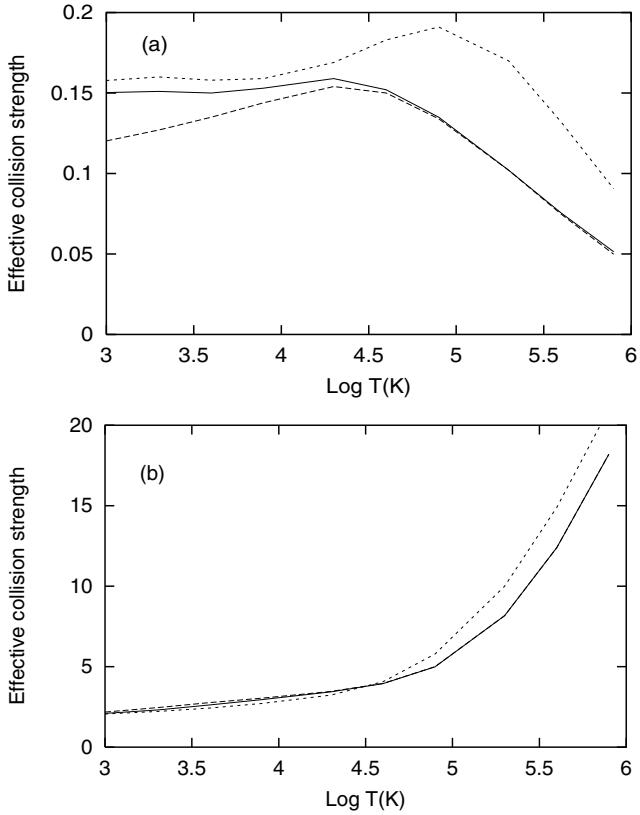

Figure 5. Effective collision strengths for excitation, from (a) the $2s^2\ ^1S$ ground term and (b) the $2s2p\ ^3P$ metastable term, to the $2s3d\ ^3D$ upper term. The dotted curves are from the present 20CC R-matrix calculation, the solid curves are from the present 114CC RMPS calculation, and the dashed curves are from the present 134CC RMPS calculation.

we see a smaller spread of results. Even so, the apparent lack of prior results for B^+ in the literature has meant that spectroscopic modelling for B^+ has taken place with effective collision strengths determined from plane-wave Born calculations (O'Mullane 2002). The plane-wave Born results for excitation from the ground term (not shown) are between a factor of 12.5 and 2.7 larger than our RMPS results over the temperature range shown, including a factor of 10.2 at 4×10^4 K.

The results for the above transitions do not mean that all transitions, from $n = 2$ to 3, show small effects due to coupling to the continuum. In figure 5, for excitation of the $2s3d\ ^3D$ term, we see that the effective collision strength is reduced significantly above $\sim 3 \times 10^4$ K. Again, the low temperature ($T \sim 10^3$ K) difference for the ground state is due to changes in the near-threshold resonance structure arising from the two RMPS calculations. Convergence has not been established here. Plane-wave Born results from the metastable term (not shown) are between a factor of 6.6 and 1.4 larger than the RMPS results over the temperature range shown, including a factor of 3.5 at $\sim 4 \times 10^4$ K.

4.3. Within $n = 2$

We do not expect to see substantial differences between results from our various calculations for transitions within the ground complex. Excitation from the ground term $2s^2\ ^1S$ to the

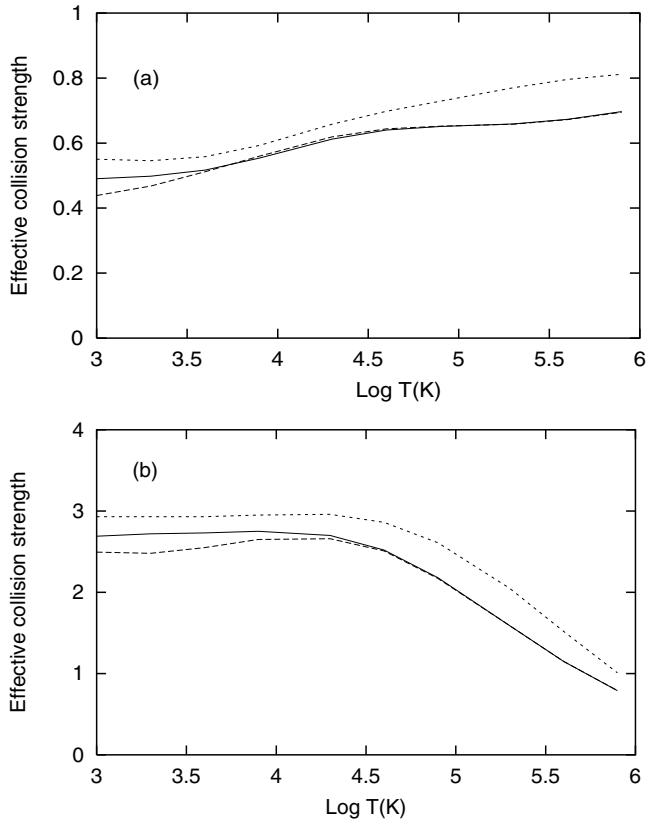

Figure 6. Effective collision strengths for excitation, from (a) the $2s^2\ ^1S$ ground term and (b) the $2s2p\ ^3P$ metastable term, to the $2p^2\ ^1D$ upper term. The dotted curves are from the present 20CC *R*-matrix calculation, the solid curves are from the present 114CC RMPS calculation, and the dashed curves are from the present 134CC RMPS calculation.

$2p^2\ ^1D$ term involves a two-electron jump. Radiation from this upper state is also observed at TEXTOR. In figure 6, we see that there is a similar spread between our results from the ground and the $2s2p\ ^3P$ metastable terms, even though excitation from the metastable involves a one-electron jump, with exchange. A modest reduction in the effective collision strengths due to continuum coupling is noted over a broad range of temperatures.

Last, but not least, in figure 7 we present results for the excitation of the metastable term from the ground term. This is the driving reaction that populates the metastable in a dynamic plasma. The accuracy of this excitation rate is thus key to the accuracy of excited-state populations driven from the metastable. We observe close agreement between our three sets of results, especially between the pseudo-state results.

4.4. Data assessment

Firstly, all low-temperature effective collision strengths are sensitive to changes in the near-threshold resonance structure, below $\sim 5 \times 10^3$ K, and uncertainties can be $\sim$40%. Our use of high-energy limit values means that our high temperature effective collision strengths should not be any more uncertain than at lower temperatures, except perhaps for spin-forbidden transitions. Based on comparisons of results from our four collision calculations, we estimate the uncertainty of our effective collision strengths to be 10–20% for dipole transitions, $\sim$20%

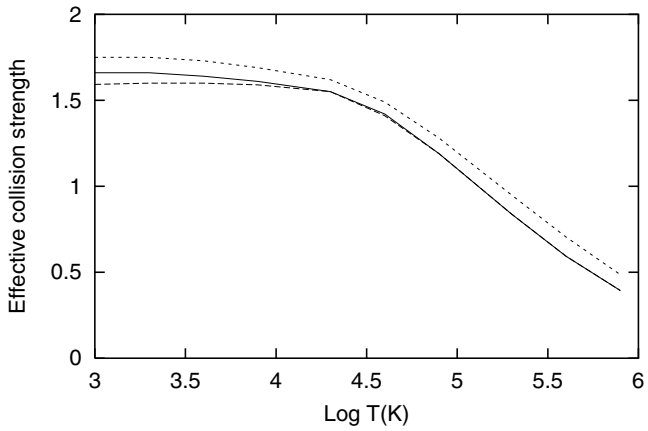

Figure 7. Effective collision strengths for excitation from the $2s^2\ ^1S$ ground term to the $2s2p\ ^3P$ metastable term. The dotted curve is from the present 20CC *R*-matrix calculation, the solid curve is from the present 114CC RMPS calculation, and the dashed curve is from the present 134CC RMPS calculation.

for non-dipole spin-allowed transitions and ∼30% for spin-forbidden transitions. The usual caveats apply to transitions that can only take place through, or which are very sensitive to, mixing.

Finally, in order to provide data for use in collisional–radiative modelling, we have generated effective collision strengths from our 114CC RMPS calculation for all possible transitions between the lowest 20 terms of B^+ for temperatures between 8×10^2 and 8×10^5 K. These collisional data, along with energy levels, electric-dipole radiative rates and Born limits, are tabulated in the ADAS *adf04* format (Summers 1999) and are available from the Oak Ridge National Laboratory (ORNL) Controlled Fusion Atomic Data Center (CFADC) website[5].

5. Conclusions

We have completed 114CC and 134CC RMPS calculations for the electron-impact excitation of B^+. The resulting effective collision strengths appear to be well converged with respect to the pseudo-state expansion, especially at higher temperatures. A comparison of these RMPS results with those from a 20CC non-pseudo-state *R*-matrix calculation shows the large effect of coupling to the continuum on effective collision strengths—reductions of up to a factor of 2. Large low-temperature enhancements, especially for transitions to $n = 4$, due to resonances attached to $n \geqslant 5$ were observed. However, due to differences in the resonance structures, the effective collision strengths from the two RMPS calculations are somewhat less well converged at the low temperatures.

It is clear that data for all light elements ($Z < 10$), from neutrals to a few times ionized, need to be reassessed for application to fusion (and, indeed, astrophysics). Such a reassessment has already been made for many H- and Li-like ions, and their neutrals, and is being extended to He-like ions. Work has only just started on Be-like ions and even here the computational effort required is significantly greater. To extend the work to B-like, C-like ions etc, and their neutrals, is important. However, even with the use of our parallel *R*-matrix suite on massively parallel computers, this remains a challenge.

[5] http://www-cfadc.phy.ornl.gov/data_and_codes

Acknowledgments

In this work, DCG was supported by a US DoE grant (DE-FG02-96-ER54367) with Rollins College and DMM was supported by a subcontract with Los Alamos National Laboratory. All calculations were performed on a 16-processor SGI Origin 300 funded through an EPSRC JREI award to the University of Strathclyde.

References

Anderson H, Ballance C P, Badnell N R and Summers H P 2000a *J. Phys. B: At. Mol. Opt. Phys.* **33** 1255–62
Anderson H, Ballance C P, Badnell N R and Summers H P 2000b *J. Phys. B: At. Mol. Opt. Phys.* **35** 1613–15
Badnell N R 1997 *J. Phys. B: At. Mol. Opt. Phys.* **30** 1–11
Badnell N R and Gorczyca T W 1997 *J. Phys. B: At. Mol. Opt. Phys.* **30** 2011–19
Ballance C P, Badnell N R and Smyth E 2003a *J. Phys. B: At. Mol. Opt. Phys.* submitted
Ballance C P, Badnell N R, Griffin D C, Loch S D and Mitnik D M 2003b *J. Phys. B: At. Mol. Opt. Phys.* **36** 235–46
Bartschat K, Hudson E T, Scott M P, Burke P G and Burke V M 1996 *J. Phys. B: At. Mol. Opt. Phys.* **29** 115–23
Borodine D 2002 private communication
Bray I, Burgess A, Fursa D V and Tully J A 2000 *Astron. Astrophys. Suppl. Ser.* **146** 481–98
Bray I and Stelbovics A T 1992 *Phys. Rev. Lett.* **69** 53–6
Burgess A 1974 *J. Phys. B: At. Mol. Phys.* **7** L364–7
Burgess A, Hummer D G and Tully J A 1970 *Phil. Trans. R. Soc.* A **266** 225–79
Burgess A and Tully J A 1992 *Astron. Astrophys.* **254** 436–53
Fernley J A, Hibbert A, Kingston A E and Seaton M J 1999 *J. Phys. B: At. Mol. Opt. Phys.* **32** 5507–22
Gorczyca T W, Robicheaux F, Pindzola M S, Griffin D C and Badnell N R 1995 *Phys. Rev.* A **52** 3877–88
Griffin D C, Badnell N R and Pindzola M S 2000 *J. Phys. B: At. Mol. Opt. Phys.* **33** 1013–28
Griffin D C, Mitnik D M, Colgan J and Pindzola M S 2001 *Phys. Rev.* A **64** 032718(6)
Jönsson P, Froese Fischer C and Godefroid M R 1999 *J. Phys. B: At. Mol. Opt. Phys.* **32** 1233–45
Mazzotta P, Mazzitelli G, Colafrancesco S and Vittorio N 1998 *Astron. Astrophys. Suppl. Ser.* **133** 403–9
Mitnik D M, Griffin D C and Badnell N R 2001 *J. Phys. B: At. Mol. Opt. Phys.* **34** 4455–73
Mitnik D M, Griffin D C, Ballance C P and Badnell N R 2003 *J. Phys. B: At. Mol. Opt. Phys.* **36** 717–30
O'Mullane M G 2002 private communication
Seaton M J 1953 *Proc. R. Soc.* A **218** 400–16
Summers H P 1999 *ADAS User Manual Version 2.1* webpage http://adas.phys.strath.ac.uk
Tully J A, Seaton M J and Berrington K A 1990 *J. Phys. B: At. Mol. Opt. Phys.* **23** 3811–37
Whiteford A D, Badnell N R, Ballance C P, O'Mullane M G, Summers H P and Thomas A L 2001 *J. Phys. B: At. Mol. Opt. Phys.* **34** 3179–91
Zhu X-W and Chung K T 1995 *Phys. Scr.* **52** 654–64